Biosensors and Bioelectronics 146 (2019) 111581

Contents lists available at ScienceDirect

Biosensors and Bioelectronics

journal homepage: www.elsevier.com/locate/bios

Thermally stable and uniform DNA amplification with picosecond laser ablated graphene rapid thermal cycling device

Zhao-Chi Chen[a], Tien-Li Chang[a,*], Ching-Hao Li[b], Kai-Wen Su[c], Cheng-Che Liu[d,**]

[a] Department of Mechatronic Engineering, National Taiwan Normal University, Taipei, Taiwan, ROC
[b] Department of Physiology, School of Medicine, Graduate Institute of Medical Sciences, College of Medicine, Taipei Medical University, Taipei, Taiwan, ROC
[c] Integrated Science, University of British Columbia, Columbia, Canada
[d] Graduate Institute of Physiology, National Defense Medical Center, Taipei, Taiwan, ROC

ARTICLE INFO

Keywords:
Thermal stability and uniformity
Thin-film device
Graphene
DNA amplification
PCR device
Picosecond laser ablation

ABSTRACT

Rapid thermal cycling (RTC) in an on-chip device can perform DNA amplification *in vitro* through precise thermal control at each step of the polymerase chain reaction (PCR). This study reports a straightforward fabrication technique for patterning an on-chip graphene-based device with hole arrays, in which the mechanism of surface structures can achieve stable and uniform thermal control for the amplification of DNA fragments. A thin-film based PCR device was fabricated using picosecond laser (PS-laser) ablation of the multilayer graphene (MLG). Under the optimal fluence of 4.72 J/cm^2 with a pulse overlap of 66%, the MLG can be patterned with arrays of 250 μm^2 hole surface structures. A 354-bp DNA fragment of VP1, an effective marker for diagnosing the BK virus, was amplified on an on-chip device in less than 60 min. A thin-film electrode with the aforementioned MLG as the heater was demonstrated to significantly enhance temperature stability for each stage of the thermal cycle. The temperature control of the heater was performed by means of a developed programmable PCR apparatus. Our results demonstrated that the proposed integration of a graphene-based device and a laser-pulse ablation process to form a thin-film PCR device has cost benefits in a small-volume reagent and holds great promise for practical medical use of DNA amplification.

1. Introduction

Polymerase chain reaction (PCR) has played a major role in genetic analysis since its discovery by Mullis et al., in 1983 (Saiki et al., 1988). Nowadays, PCR is an integral tool of modern biotechnology processes and biological identification. Due to the growing demands of on-site diagnosis in medicine, the realization of point-of-care (POC) PCR strategies has garnered much attention (Petralia and Conoci, 2017). PCR has dramatically enhanced the detection of low levels of pathogens by amplifying their dedicated deoxyribonucleic acid (DNA) fragment with high precision and accuracy (Jaenisch and Bird, 2003). Several million copies of DNA can be generated from a single molecule through only few cycles of PCR. Thus, PCR has been used for diagnosing many infectious diseases, such as HIV (Mackay et al., 2002), the coronavirus genus (Drosten et al., 2003; Huang et al., 2018), Epstein–Barr virus (Yamamoto et al., 1995), and eubacterial (Hryniewiecki et al., 2002; McCabe et al., 1995) and *Escherichia coli* infections (Holland et al., 2000; Kim et al., 2018). In principle, this method can be applied to other taxonomic groups of pathogens (e.g., families, genus, species of viruses, bacteria, and fungi) by designing a broad-range PCR assay (Evertsson et al., 2000). DNA amplification is performed using thermal cycling, with a high degree of control of stable and uniform temperature distribution being attributed to array structures (Bigham et al., 2017; Seo et al., 2018), microchannel heat exchangers (Riera et al., 2013), membrane-based microfluidics (Chen and Shen, 2017), and doped hybrid materials (Seo et al., 2016). Bigham et al. (2017) demonstrated a novel measurement technique where the heat and mass transfer process was analyzed within surface structures with unprecedented detail. Useful pillars occupied a narrow range between 0.5 and 10 μm, with the optimum at 2 μm, thus illustrating the challenges of enhancing surface heat transfer through the incorporation of surface array patterns in a microstructure with high heat and mass flux in the absence of the types of microscale data and physical insights provided here.

A graphene-based material is promising as a candidate platform for biosensors because of its high surface-area-to-volume ratio, excellent

* Corresponding author. Department of Mechatronic Engineering, National Taiwan Normal University, 162, Sec. 1, Ho-Ping E. Road, Taipei, 106, Taiwan, ROC.
** Corresponding author.
E-mail addresses: tlchang@ntnu.edu.tw (T.-L. Chang), jasonliu@mail.ndmctsgh.edu.tw (C.-C. Liu).

https://doi.org/10.1016/j.bios.2019.111581
Received 11 March 2019; Received in revised form 2 June 2019; Accepted 8 August 2019
Available online 09 August 2019
0956-5663/

conductivity, small band gap favorable for sensitive electrical and electrochemical abilities (Zang et al., 2017; García et al., 2018; Liu et al., 2018), and tunable optical properties for absorbance and reflectance such as plasmonics and fluorescence (Kim et al., 2016; Justino et al., 2017; Suvarnaphaet and Pechprasarn, 2017). In general, laser ablation enables the removal of a material without the use of lithographic masks, and other predetermined patterns commonly used in the fabrication of biosensing devices (Liébana et al., 2016; Chen et al., 2017; Verma et al., 2018). To pattern a graphene-base device, laser-ablated graphene (LAG) has been proposed as a potential fabrication method, with its selective ablation, configurability, and versatility. Lin et al. (2018) fabricated a flexible, highly sensitive non-enzymatic glucose sensor by using DVD laser patterned graphene as a flexible conductive substrate. This glucose sensor demonstrated excellent catalytic activity for glucose oxidation and a linear glucose detection range from 1 μM to 4.54 mM, with a high sensitivity and a low detection limit (0.35 μM). Vanegas et al. (2018) reported the development of LAG electrodes by using locally sourced materials for reagent-free food safety biosensing. This amperometric biosensor exhibited satisfactory electrochemical performance, with an average histamine sensitivity of 23.3 μA/mM, a lower detection limit of 11.6 μM, and a response time of 7.3 s for biogenic amines. Cardoso et al. (2019) proposed an ultrasensitive biosensor using a method of laser-induced graphene to perform the patterned electrodes. The porous multilayer graphene structures were produced on a polyimide (PI) substrate and showed a resistivity of 102.4 ± 7.3 Ω/square. Based on the cyclic voltammetry (CV) and electrochemical impedance spectroscopy, the detection limit for chloramphenicol at redox was 0.62 nM where the linear response range was controlled from 1 nM to 10 mM.

The use of graphene film has dominated the printed electrode technique for biomedical devices (Du et al. 2010; Cheng et al., 2016; Liébana et al., 2016). However, the patterning area and complexity in graphene-based fabrication require considerable improvement in the quality of laser pulse machining. Compared with the conventional laser technologies, the ultrafast laser processing (e.g., picosecond or femtosecond laser) with the minimal heat affected zone has particular advantages of high efficient and precise for micromachining (Sugioka and Cheng, 2014; Chang et al., 2016). This type of laser has a short pulse duration and high peak power intensity, which can induce the nonlinear absorption in the material during irradiation and offers the advantages of more precise resolutions (Chen and Chang, 2015). As a result, the ablated structures and devices will obtain higher efficiency and better flexibility after ultrafast laser micromachining without the need for post-processing (Rethfeld et al., 2017; Winter et al., 2017). Additionally, the thermal diffusion to the laser-ablated around the area is very limited (i.e., the ultrafast excitation only occurs within the focal spot), which can be a very attractive feature of high-resolution ultrafast laser processing of graphene films.

BK virus (BKV), a human polyomavirus, is a non-enveloped double-stranded DNA virus with an approximately 5000-base-pair circular genome that encodes structural proteins (VP-1, -2, and -3) and regulatory agnoprotein (Ahsan and Shah, 2006). BKV is widely recognized as a major cause of kidney transplant dysfunction and subsequent allograft failure. Moreover, this virus may remain latent in the epithelial cells of the renal tubule which eluding detection until the infected cells of a patient with BKV nephropathy undergo lysis, the BKV detection is one of most urgent issue for the clinical patients of renal transplantation (Yin et al., 2015; Shenagari et al., 2017; Jha et al., 2018; Tan et al., 2019). The virus leaks into the renal tubular lumen, showing a viral titer of 10^5 to 10^7 copies/mL in urine (Hirsch et al., 2005; Gjoerup and Chang, 2010; Barraclough et al., 2011). Currently, a PCR-based method is still the most frequently applied technique for detecting viral DNA in urine for clinical diagnosis (Hirsch et al., 2005; Sawinski and Goral, 2015). However, this requires expensive, fixed equipment, unsuitable for field or POC applications. Therefore, it is necessary to develop an inexpensive, easy-to-use, and reliable alternative device for monitoring

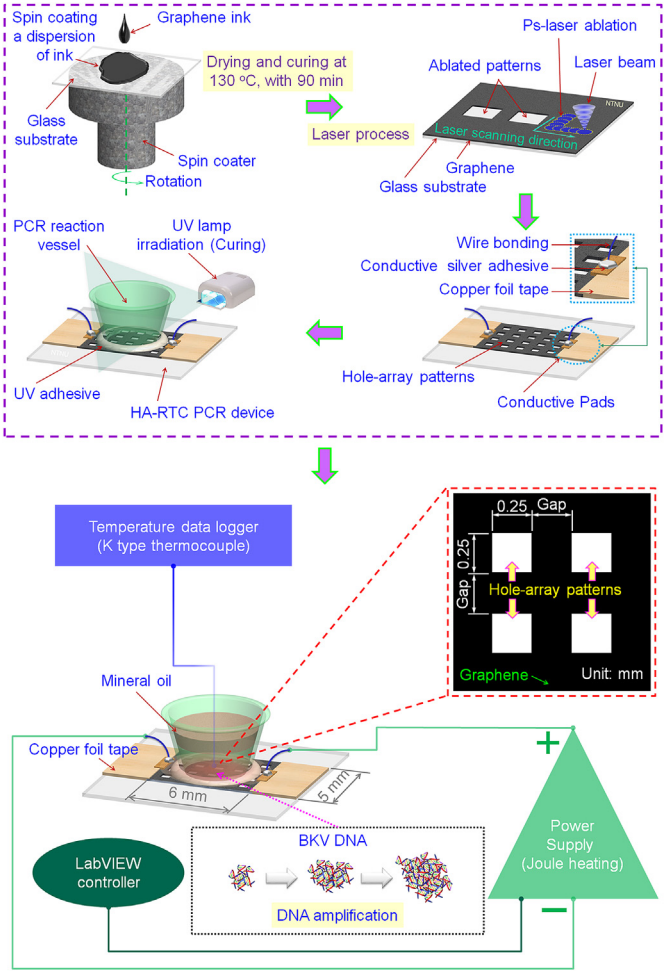

Fig. 1. Schematic illustration of the fabrication process of HA-RTC PCR device.

BKV in POC applications. To the best of our knowledge, the efficiency of PCR depends on the ability of the DNA sample to disperse, as well as the rate of thermal cycling. Compared with the different thermal cycling technologies (such as thermoelectric, photonic, electromagnetic induction and microwave), the method utilizing Joule heating in rapid thermal cycling is easy to integrate with the PCR device (Neuzil et al., 2006; Dinca et al., 2009; Lien et al., 2009; Ugsornrat et al., 2010). The thermal device of Joule heating utilizing LAG technique has been fabricated with high stability and good thermoelectric conversion efficiency in our previous studies (Chang and Chen, 2015; Chang et al., 2016).

Most researchers have very little experience in studying for the topics of DNA amplification by Joule heating. This is the first study to report an alternative BKV detection method by using a graphene-based device as a microheater and a LAG technique for DNA amplification, in which the LAG technique can provide Joule heating and hydrophilic surface characteristics to improve the efficiency of PCR. Because graphene interacts extremely well with DNA templates or primers, it may also enhance PCR specificity (Liu et al., 2016). The addition of graphene improves the formation of a matched primer template complex, suppresses a mismatched complex, and favors PCR amplification (Jia et al., 2012; Wang et al., 2017; Chen, 2018). Therefore, the unique electro-thermal properties of picosecond laser (PS-laser) patterned multilayer graphene (MLG) with the mechanism of surface structures can provide the excellent on-chip sensing device for BKV DNA amplification. The suitability of these laser patterned MLG thin-film electrodes was the one-step manufacturing process for being tested with PCR thermocycling. Thereby, the stable and uniform temperature

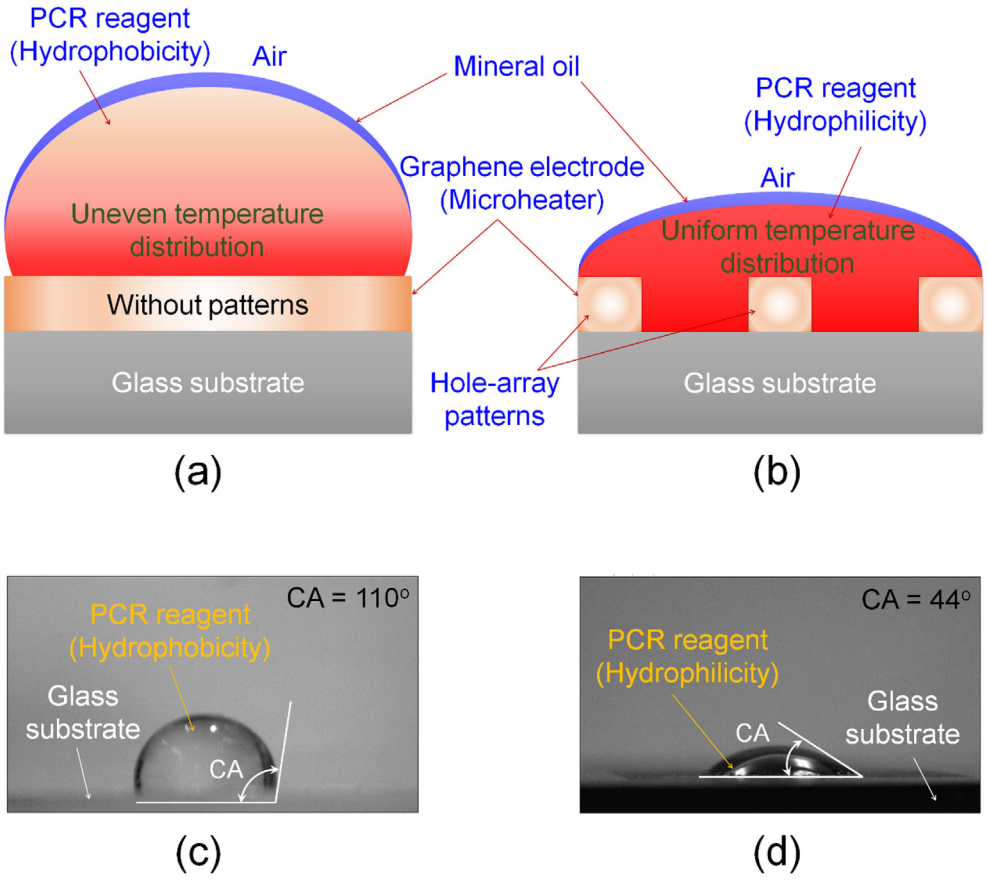

Fig. 2. Schematic of the HA-RTC PCR device with stable and uniform temperature distribution: (a) The hydrophobic surface of the spin-coated graphene. (b) The hydrophilic surface of the graphene electrodes with hole-array structures. (c) CA measurement for image of the hydrophobic surface of the spin-coated graphene. (d) CA measurement for image of the hydrophilic surface of the graphene electrodes with hole arrays structures.

distribution was reported throughout all temperature ranges covering template denaturation, primer annealing, and extension. Herein LAG technique has the ability to precisely and fast ablate the design of tiny graphene electrodes for forming the temperature-control device, which can be developed into portable devices and used in small handheld devices for DNA amplification, and even for preventive biomedical applications, such as identification of antibacterial or antagonistic activity of probiotics (Fijan et al., 2018; Karimi et al., 2018).

2. Materials and methods

2.1. Materials and equipments

The MLG thin-film formed by graphene ink (model: I-MS18, Enerage Inc., Taiwan). The programmable picosecond laser ablation system (PS-laser, model: Awave-532 nm Series Laser, Advanced Optowave Co., Ltd., USA). The copper foil tape (model: 3313, 3 M, USA). The conductive silver adhesive (model: OP-901, Double-O Technology Co., Ltd., Taiwan). Wire bonded by a soldering tin (lead-free solder wire, model: W3050 RMA, Ku Ping Enterprise Co., Ltd., Taiwan). The PCR reaction vessel (microcentrifuge tube, model: MB-P02, Gunster Biotech Co., Ltd., Taiwan). The UV adhesive (model: 5801, LOCTAI Enterprise Co., Ltd., Taiwan). The power supply (model: GPC-6030D, GW Instrument Co., Ltd., Taiwan). The K-type thermocouple (model: midi Logger GL240, Graphtec, Japan). The ultrapure water (ultrapure water purification system, model: Milli-Q Integral, Merck Ltd., Taiwan). The mineral oil (model: 69797, Sigma-Aldrich, Inc., Taiwan). The LabVIEW controller (Version 2015 SP1, National instrument Company, USA). The BKV was isolated from a patient's urine (IRB No. 1-102-05-124, NDMC, Taiwan), and cultured using Vero cell (ATCC CCL-81, Bioresource Collection and Research Center, Taiwan). The buffer-based DNA extraction kit (TX-CD01, TOOLS, Taiwan). The invitrogen platinum PCR SuperMix and high fidelity product were purchased from Life Technologies Corporation in Taiwan. The UV spectrometer (model: GeneQuant 1300, GE Healthcare Life Science, USA). The characteristics of HA-RTC PCR device were analyzed by scanning electron microscopy (SEM; model: Helios NanoLab 1200+, FEI, USA), thermal imager (model: KT-80, Sonel, Poland) and ImageJ software (version 1.52c, National Institutes of Health, USA). The electrophoresis of genomic BKV DNA was analyzed by using agarose gel (No. 15628019, Thermo Fisher Scientific, Inc., USA) and electrophoresis cell (model: MT-108, Major Science, Taiwan).

2.2. Design and fabrication of PCR device

The fabrication process of a hole-array rapid thermal cycling (HA-RTC) PCR device is illustrated in Fig. 1. The HA-RTC PCR device included a two-layer stack consisting of a soda-lime glass substrate and an MLG thin film. First, a glass was cut into dimensions of 6 mm × 5 mm × 0.4 mm by using a diamond knife, and this glass was used as an HA-RTC PCR device substrate; sequentially, it was cleaned using acetone, isopropanol, and deionized water for 5 min through ultrasonication. Graphene ink was applied to homogeneous MLG thin films on a 0.4-mm-thick glass substrate model by using a two-step spin-coating process (3000 rpm and 4500 rpm for 20 s each). To remove organic solvents from graphene ink, the MLG thin film was heated at 130 °C at 90 min for curing and drying. After an MLG thin film had formed on the glass substrate, hole arrays patterned on the thin-film layer were ablated using a programmable picosecond laser writing directly to form graphene electrodes for HA-RTC device. The graphene electrodes consisted of hole arrays where the electrode size of both square and gap were 250 μm. The dimensions of HA-RTC device were 6 mm in length, 5 mm in width, and 0.4 mm in height. And the effective heating area of device were 2.75 mm length 2.25 mm in width, and

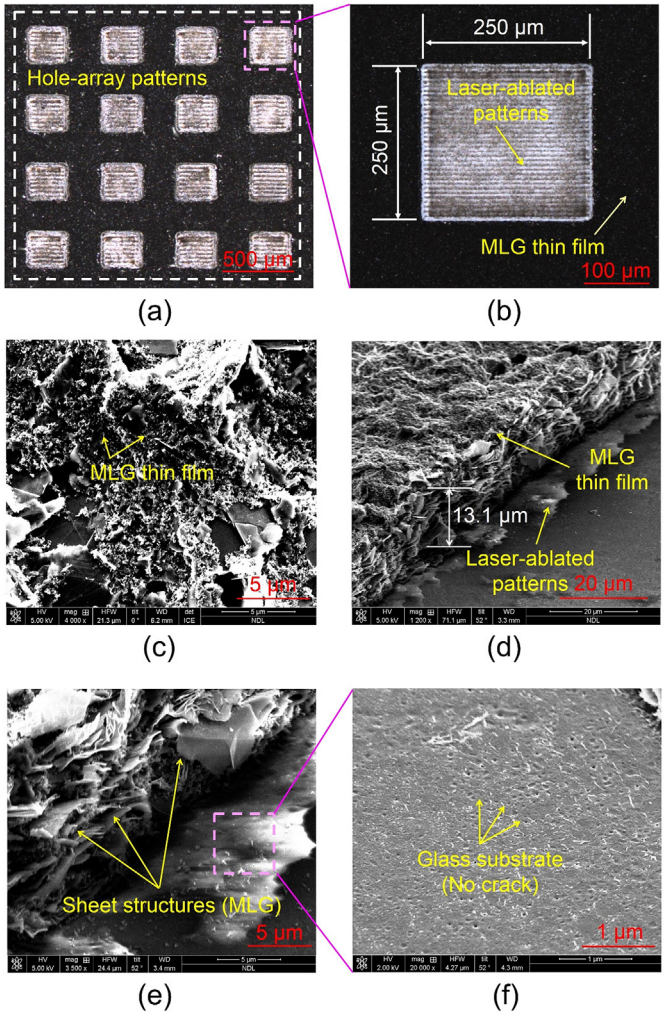

Fig. 3. (a, b) LSCM images of 4 × 4 hole-array patterns of MLG thin film on glass substrate. (c) SEM image of MLG thin-film surface morphologies and locally magnified multilayer graphene structures. (d) SEM image of laser-ablated edge patterns of MLG thin film on glass substrates and its enlarged images (e, f).

13 μm in height. The MLG thin film/glass was attached to a copper foil tape, conductive silver adhesive, and wire bonding with a soldering tin to form conductive pads. Next, the PCR reaction vessel was attached to the MLG thin-film surface by using a UV adhesive fixed with a UV lamp exposing bonding surface interfaces for surface curing. Finally, a power supply was connected to two conductive pads. And a K-type thermocouple was measured with the tip of probe to monitor the heating temperature when installed PCR reaction vessel. After the PCR reaction vessel was filled with BKV culture, PCR reagents, ultrapure water, and mineral oil, the HA-RTC PCR device was operated using LabVIEW. The power supply offered a stable voltage of 25-V, 18-V and 22-V outputs for heating the surface during DNA amplification in 30 cycles using the LabVIEW system controller.

2.3. PCR device fabrication

The PS-laser hole-array patterning technique for fabricating an HA-RTC device was based on the ablation of the MLG thin film spin-coated on the glass substrate. The PS-laser setup for fabricating the graphene electrodes consisted of a diode-pumped solid-state laser operating at 532 nm combined with a galvanometric scanner system for the output laser beam. The electrode structures were formed by the laser average power in range of 0.9–2.5 W based on the corresponding to the threshold fluence in range of 2.45–4.72 J/cm^2 with 7 ± 2 ps pulse duration. Here, the optimal laser parameters of average power, repetition rate, and scanning speed were 2.5 W, 300 kHz, and 500 mm/s, respectively. The beam was focused by the F-Theta lens with a focal length of 105 mm that provided a uniform irradiance distribution over a working area of 60 × 60 mm^2. The laser-obtained beam spot size using this F-θ lens, determined at 1/e^2 of the Gaussian profile (beam quality factor $M^2 < 1.3$) was 15 μm. To fabricate graphene electrodes, the laser beam was focused on the surface of the MLG thin-film layer. At a laser fluence below the damage threshold of the glass substrate (4.72 J/cm^2) and above the ablation threshold of the MLG thin film (2.45 J/cm^2) with a pulse overlap of 66%, the selective MLG thin-film layer according to the graphene-based electrode design can be removed. The CCD camera and LED light were installed to in-situ monitor the PS-laser process.

2.4. Virus culture and PCR reagents

BKV used in this experiment was a gift from Dr. Liu Cheng-Che (Department of Physiology, National Defense Medical Center, Taipei, Taiwan.). The cultured BKV budded in the medium of infected Vero cell on the 19th day, and the supernatant was collected for the following tests. Viral DNA was extracted using a buffer-based DNA extraction kit. The Invitrogen Platinum PCR SuperMix, High Fidelity product and primers that used in this experiment were specifically selected to amplify 354-bp BKV VP1 fragments (Jin, L. 1993; Krumbholz et al., 2006; Sawinski and Goral, 2015). They were synthesized by Genomics Bioscience and Technology Corporation (Taiwan), and using the following sequences: 5′-AAGTTCTAGAAGTTAAAACTGGG-3′ (forward) and 5′-GTGGAAATTACTGCCTTGAATAGG-3′ (reverse). The reagent mixture for the PCR reaction (25 μL) was composed of 13 μL of Platinum PCR SuperMix, 1 μL of each primer, 3 μL of BKV genomic DNA and 8 μL of ultrapure water. Herein the mineral oil can be the fixed volume (2.5 μL). Except mineral oil, the final volume of each reaction was 25 μL for the sample, in which the concentration of BKV DNA was adjusted by varying the volume of ultrapure water. The optical density of genomic BKV DNA was quantified using a UV spectrometer. The initial genomic BKV DNA content varied from 1.5 × 10^{-5} pg/copies (equivalent to 4.8 × 10^5 genomic copies/sample) to 5 × 10^{-6} pg/copies (equivalent to 1.6 × 10^5 genomic copies/sample).

2.5. Characterization

The surface morphology of formed graphene electrodes on the HA-RTC PCR device was characterized through scanning electron microscopy. The thermal image of the HA-RTC PCR device was captured using a thermal imager. The band brightness of gel electrophoresis was analyzed using the open-source ImageJ software. The genomic BKV DNA was then mixed with 2 μL of buffer and analyze through gel electrophoresis with 1% agarose gel at 100 V for 30 min, together with a 100-bp DNA ladder.

3. Results and discussion

3.1. DNA amplification by PCR device

Fig. 2 shows the operation of HA-RTC PCR device with the aforementioned stable and uniform temperature distribution. Preliminary experimentation employing the RTC microheater was performed. PCR efficiency is affected by interactions between the device surface, and the biomolecules in the PCR solution (including mineral oil of identical temperature for the sample as a reaction mixing overlay). Due to the mechanism of surface structures on PCR device, suitable surface treatment is required to ensure the success of PCR on-chip device for DNA amplification (Gong et al., 2006). Considering that the increased heat transfer on the device can facilitate thermal equilibrium, the reaction time could further be reduced. Due to the hydrophobicity of the spin-

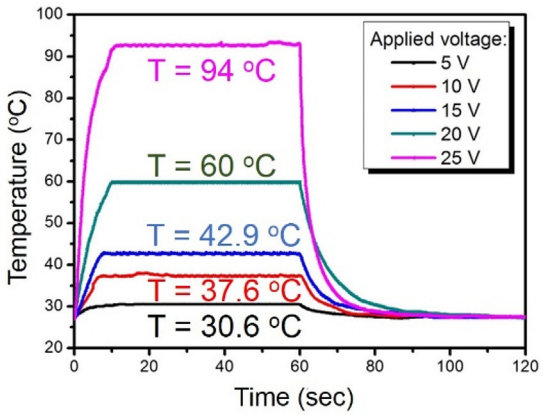

(a)

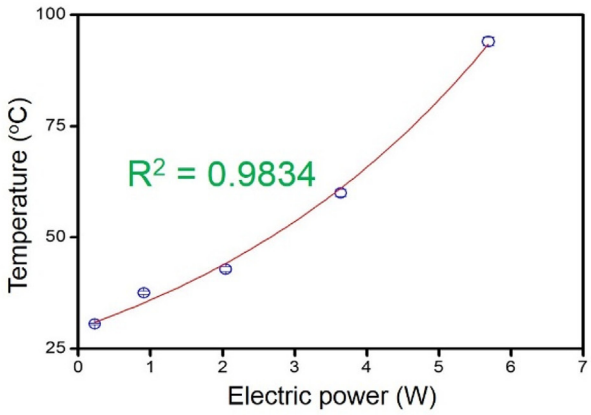

(b)

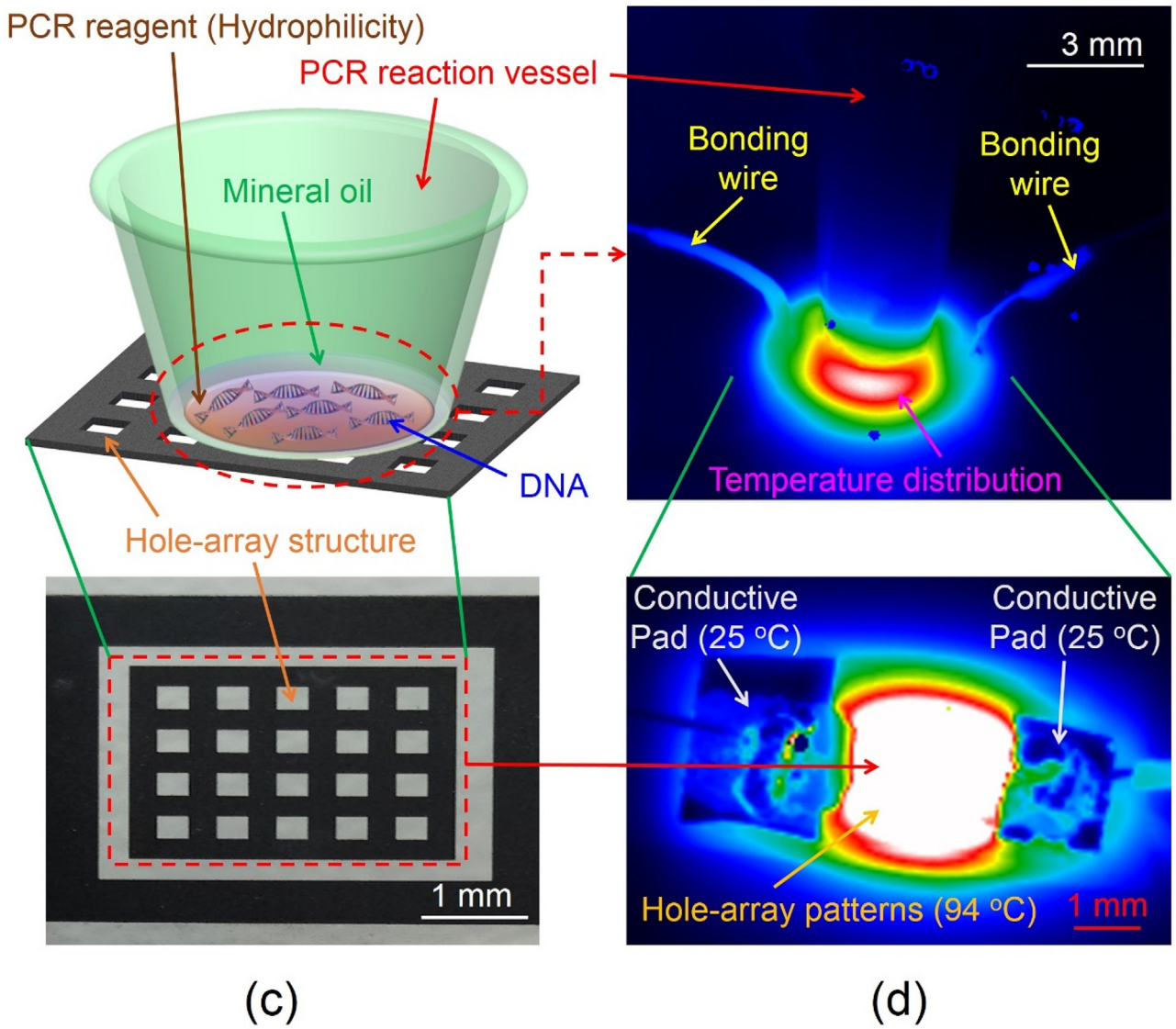

(c) (d)

Fig. 4. (a) Time-dependent temperature changes in the MLG thin-film structure at various applied voltages from 5 to 25 V. (b) Steady-state temperature of the MLG thin film as a function of electric power with applied voltage. (c) A typical digital image of the MLG thin film after PS-laser hole-array patterning. (d) The MLG thin film (PCR device) can be used with an applied voltage of 25 V for electric heating experiments where the infrared thermal image of the DNA amplification at the temperature is 94 °C.

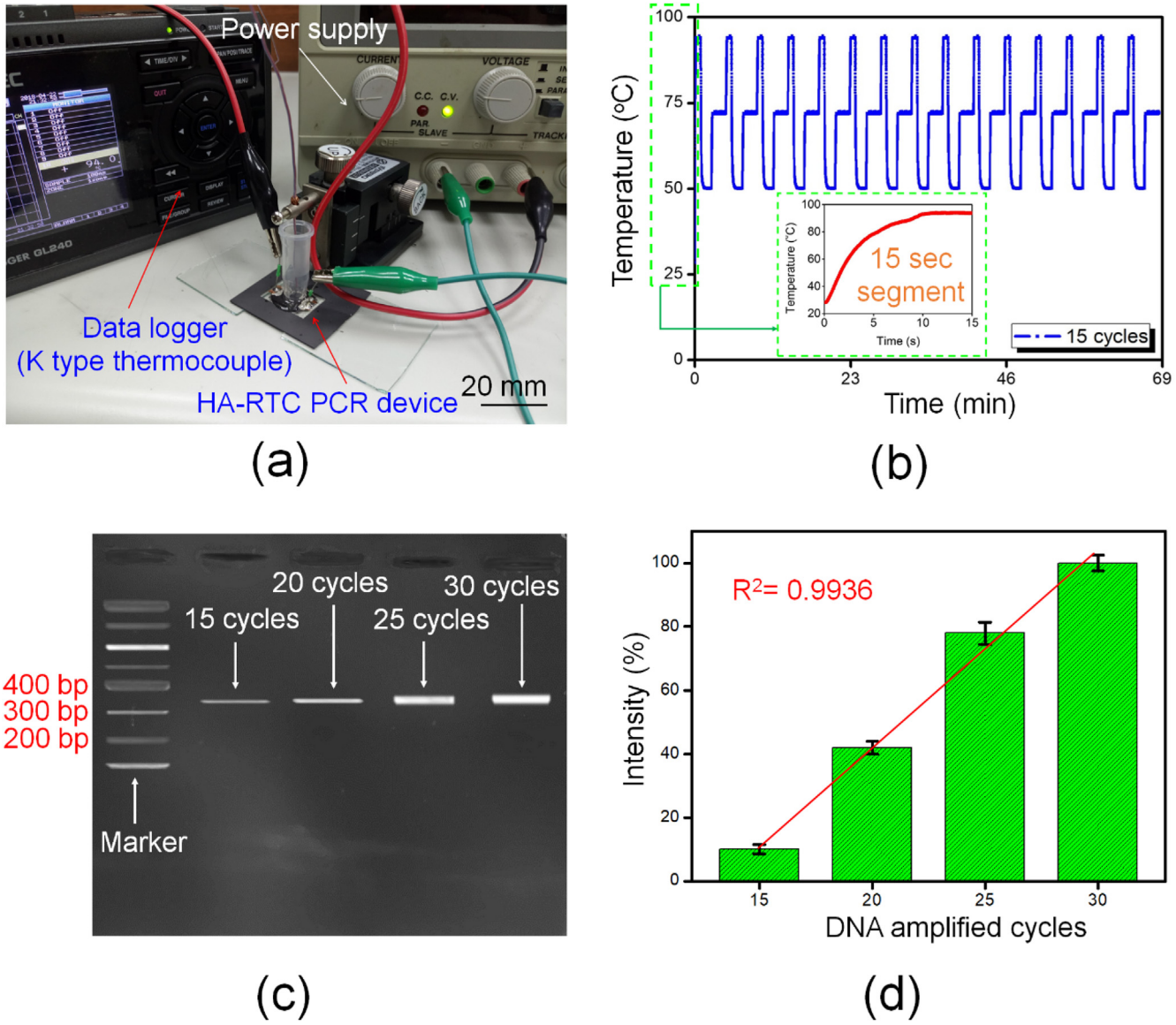

Fig. 5. (a) Experimental setup with power supply and data logger for testing the HA-RTC PCR device for DNA amplification. (b) Relationship obtained by applying a thermal cycle of 94 °C, 50 °C, and 72 °C for 15 cycles with a duration of 40, 60, and 120 s, respectively; a 15-sec segment is shown. Verification of the HA-RTC PCR device is shown in (c). (d) The resulting calibration curve of different DNA amplified cycles. Bar plots represent mean ± S.D. from 3 independent detections.

coated graphene thin film, the PCR reagent has a large contact angle (CA) and height, as shown in Fig. 2a. Fig. 2b shows the hydrophilic surface of a graphene electrode having a hole arrays structure, the lower droplet height and CA enabling more heat flux and thermal conductivity during heating, thereby improving thermal efficiency. (Crafton and Black, 2004; Wu et al., 2016; Hänichen et al., 2019). In this study, the spin-coated graphene with the CA of 110 ± 1° was measured that thin-film device surface (Fig. 2a) was hydrophobic, as shown in Fig. 2c. After forming the graphene electrodes with hole arrays structures (Fig. 2b), the structure property of PS-laser-ablated surface on thin-film device can be the hydrophilic surface where CA was 44 ± 1°, as shown in Fig. 2d. These binary structures of the hole-array patterns and the MLG sheets have demonstrated the wetting characteristics of the material surface, which can indicate that HA-RTC PCR device has wettability gradient surface (Li et al., 2016; Ngo and Chun, 2017). PS-laser ablated patterns of hydrophilic surface permitted wettability modification of a hydrophobic surface (graphene layer). The ablated surface can generate the required surface tension gradient for the design of PCR device for DNA amplification. The temperature monitoring and microheater inside the PCR device along a programmable controller were used to form a temperature control module, which can perform the precise on-chip platform of PCR thermal cycling. Finally, the detecting gene for BKV was amplified and detected.

3.2. Surface morphology of the graphene-based device by picosecond laser pulses

The surface morphologies of the MLG thin film and glass substrate of the HA-RTC device were measured using LSCM and SEM. Fig. 3a shows the micrographs of laser ablation with a fluence of 4.72 J/cm^2, a repetition rate of 300 kHz, and a scanning speed of 500 mm/s to form the hole-array patterns of MLG thin film on the glass substrate, which can be measured using LSCM. These patterned MLG thin films were uniform and smooth, and the ablated patterns had sharp corners and straight edges, as shown in Fig. 3b. Fig. 3c shows the surface structures of the MLG thin film on a glass substrate measured using SEM. The exposed graphene sheets at the glass substrate surface showed its multilayer characteristics, which were measured by Raman spectrum (514 nm excitation). The sharp peaks of MLG were the G band

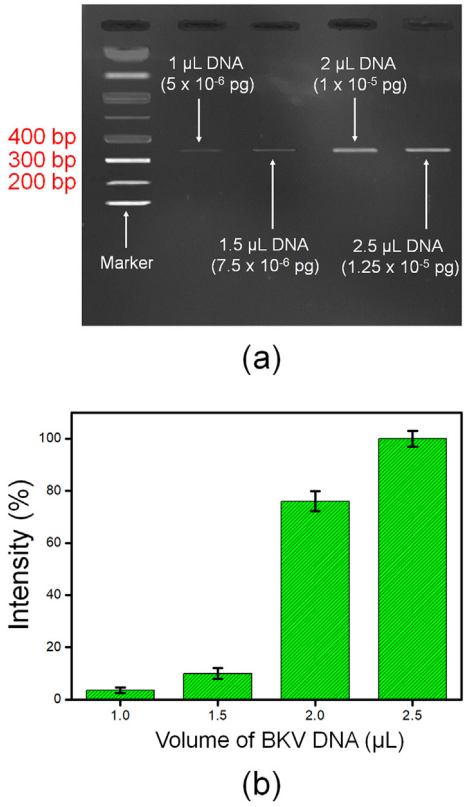

Fig. 6. (a) Gel electropherogram showing the results of the dilution test. Genomic BKV DNA in the range from 1 to 2.5 μL was thermocycled for 15 cycles, and the HA-RTC PCR device with the lowest BKV DNA content (5×10^{-6} pg/μL) produced a visible band. (b) The results of relative BKV band intensity at various volumes of BKV DNA.

($1580\ cm^{-1}$), the 2D band ($2720\ cm^{-1}$) and a low-intensity disorder-induced D band ($1354\ cm^{-1}$) (Hao et al., 2010; Chang and Chen, 2015). After this type of ultrafast laser patterning at a well-controlled low threshold fluence, the MLG thin films were completely removed and a clean edge was produced (Fig. 3d and 3e). To control-experiments of comparison between different surface structures, the laser-material interactions and subsequent material removal must be considered the damaged substrate, material residue and surface patterned structures in which the PS-laser with a non-linear mechanism can be uniquely distinct from traditional thermal ablation (Mackenzie et al., 2015; Dong et al., 2016; Chang et al., 2019). This observation proved that the laser-ablated glass substrates appeared to be without damage or incomplete residue structures, with the MLG thin films removed completely, as shown in Fig. 3f.

3.3. Graphene-based heating device with hole-array patterns

To evaluate the heating performance of the hole-array patterned graphene-based device, input voltages were supplied to the heating device through the MLG thin-film electrodes. The heating behavior of the graphene-based device as a function of time is shown in Fig. 4a. By increasing the voltage from 5 to 25 V, the steady-state temperature (thermally stable condition) reached after 60 s could be increased from 30 to 90 °C. The temperature of the MLG thin film increased rapidly when voltages above 5 V were applied, with the maximum temperatures attained within 10 s and remaining constant over time. When the applied voltage was turned off for 60 s, the temperature decreased to room temperature in less than 30 s. However, it can be found that the maximum temperature increased significantly with respect to the applied voltage increment, as shown in Fig. 4b. This growth in the maximum temperature relative to the applied voltage is consistent with temperature-electric power curves, supporting the fact that electric power is effectively transformed as heat. Moreover, the total electric power (power consumption) of the MLG thin film was formed as a heater to be calculated by basic electrical formulas. The temperature could be controlled by the electrical power P with the applied voltage to operate the heating device where the equations can be written as (Kang et al. 2011; Jung et al. 2013): $P = IV = V^2/R$. V is the applied voltage from the power supply, I is the electric current, and R is the resistance of the MLG thin film (100 Ω).

Fig. 4c shows a photograph of the laser ablated device, which can be the hole-array patterned MLG thin film for the electric heating measurement (i.e., the design of HA-RTC PCR device). With an applied voltage of 25 V, the steady-state temperature of graphene-based device momentarily increased. The infrared thermal image of the PCR device at their steady-state temperature distribution (e.g., a set temperature of 94 °C) can be shown in Fig. 4d. It should be noted that the temperature distribution of on-chip device consisted of the entire base surface of the PCR reaction vessel, thus allowing for the homogenous heating during RTC process. Thermally uniform conditions were observed in the amplified image (Fig. 4d). And it indicated that the PCR reaction vessel does not affect the temperature control of MLG microheater.

3.4. Temperature control of the HA-RTC device for PCR thermal cycling

To investigate the effect of device temperature on thermal cycling performance, measurement based on a data acquisition module and a power output control module was performed using a stable applied voltage and continuous temperature monitoring, as shown in Fig. 5a. Temperature control using a programmable HA-RTC device to obtain precise temperature rise and decay characteristics is a critical factor for successful PCR. The response characteristics of HA-RTC device were measured by applying the voltage to obtain three different temperatures of 94 (denaturation), 50 (annealing), and 72 °C (extension) for 15

Table 1
Comparison of the proposed PCR device at different fabrication techniques for DNA amplification.

Fabrication method	Material	Target	Limit of detection	Sequence (5′–3′)	Reference
LAG	MLG thin film	BK virus	5×10^{-6} pg/μL	(f) AAGTTCTAGAAGTTAAAACTGGG (r) GTGGAAATTACTGCCTTGAATAGG	This study
Electrochemical	Graphene/ZnO nanocomposite-modified SPCE	Avian influenza H5N1 virus	7.4357×10^{-6} M	(f) GGTTACCATGCAAACAACTCGACAGAGC (r) ATTGTAACGACCCATTGGAGCACATCCATAAG	Low et al.
Surface plasmon resonance	GO-AuNPs	miRNA-141	10^{-15} M	UAACACUGUCUGGUAAAGAUGG	Wang et al.
Electrostatics-driven	GO-1-PPi	Primers of C2-EGFP	6.5×10^{-8} M	(f) GAACAAGGATCCGTGAGCAAGGGCGAGGAGCT (r) CCGTAACTCGAGCGGTACAGCTCGTGCATGGC	Lee et al.
Electrochemical	p-RGO/AuNPs/CILE	Probe ssDNA	3.17×10^{-14} mol/L	NH_2-TGGCGGCACATTTGTCACTGCA	Niu et al.
Electrospinning/ microfluidic	Carbonization of SU-8 nanofiber	Salmonella	10 CFU/mL	TATGGCGGCGTCACCCGACG GGGACTTGACATTATGACAG	Thiha et al.

SU-8: SU-8 photoresist, **CFU**: Colony-forming unit, **ZnO**: Zinc oxide, **SPCE**: Screen printed carbon electrode, **GO**: Graphene oxide, **1**: Probe 1, **PPi**: Pyrophosphat, **p-RGO**: Partially reduced graphene oxide, **AuNPs**: gold nanoparticles, **CILE**: carbon ionic liquid electrode. **f**: forward, **r**: reverse, **LAG**: laser ablation graphene.

cycles in 70 min. The thermal cycle was achieved using different applied voltages of 25, 18, and 22 V corresponding to these temperatures; the relationship thus obtained is shown in Fig. 5b. The HA-RTC device's temperature increased and decreased rapidly when voltage was applied, with an extremely short rising time (10 s) from room to steady-state temperature (94 °C) (Fig. 5b, insert). And that it ended up with 30 cycles in 140 min for a final extension (the last RTC step), which can be the final phase of thermal cycling for the expected ended-point on-chip PCR. Temperature deviations of less than ± 1 °C at the annealing and extension temperature was comparable to the conventional 96-well Peltier-based thermal cyclers (Carter et al. 2010). These results demonstrated the validity of the HA-RTC device for applications such as in PCR chip and cell culturing. Through a direct technique, the rapid thermal cycling of the on-chip device could reduce the total reaction time (Moschou et al., 2014; Nieto et al., 2017).

To verify the DNA amplification on HA-RTC device, the control reactions of PCR on-chip system with 1.6×10^5 copies of genomic BKV DNA were thermocycled in a range of 15–30 cycles, as shown in Fig. 5c. It can be found that the effect of formed device on thermal performance during the thermal cycles, i.e., DNA amplification performance at different cycle numbers. The reaction droplets had a fixed volume of 25 μL, with 3 μL of target DNA, and the amplification products of the 354 bp. Moreover, the HA-RTC PCR device showed a bright target BKV DNA band that indicated well-established nucleic acid amplification. The intensity of calibration curve and the amplified cycles of BKV DNA are proportional to the increase in the number of cycles, as shown in Fig. 5d. The feasibility of a proof-of-concept in PS-laser ablated thin-film process to form a rapid thermal cycling device was performed.

3.5. HA-RTC device for DNA amplification

To determine the effectiveness of the HA-RTC PCR device, amplification on a sample with a known low DNA concentration (diluted DNA solution) was performed, as shown in Fig. 6a. For dilution tests, thermocycled reactions containing genomic BKV DNA with target volumes ranging from 1 to 2.5 μL (equivalent to 1.6×10^5 genomic copies) were used. The detection limit of the proposed method can be as low as 1 μL for BKV. Amplification was verified by gel electrophoresis: identifying band intensity in the appropriate molecular weight of 354 bp. The relative band intensity of DNA increased with the addition of 1, 1.5, 2, and 2.5 μL of genomic BKV DNA to the reagent, as shown in Fig. 6b. We observed that this produced a positive intensity ranging from 3.5% (1 μL of BKV DNA) to 100% (2.5 μL of BKV DNA). The bands are separated by molecular weight; that is, more strands of DNA of a particular molecular weight. This could be attributed to the fact that the excellent heating abilities of HA-RTC PCR device (heating rate of 13 °C/s), resulted in greater enzymatic activity in nucleic acid amplification. The dilution test results confirmed that the HA-RTC PCR device was sufficiently sensitive, with a detection limit of 5×10^{-6} pg/μL for genomic BKV DNA.

Table 1 shows a comparison of PCR devices at different fabrication techniques for DNA amplification. In terms of detection limit, the proposed HA-RTC device utilizing LAG technique can be used not only as a microheater, but also to increase the amplified concentration of genomic BKV DNA by continuous thermal control. For instance, the conventional photolithography was to be used to fabricate the PCR device, it would need complex patterned masks for each step of the process (Thiha et al., 2018). It is also well-known that the reagents for surface chemical modification through successive exchange of reactants for bio-specific detection of PCR, are still complex and not suitable for mass production (Low et al., 2016; Wang et al., 2016; Lee et al., 2017; Niu et al., 2017). To determine a one-step manufacturing process for an on-chip PCR device, this work demonstrates the feasibility of the thin-film PCR device with LAG technique for human polyomavirus diagnosis, which can achieve the detection limit of BK virus DNA to 5×10^{-6} pg/μL by way of amplification through the use of PS-laser hole arrays electrode structure patterned of MLG thin film.

4. Conclusions

In this study, an HA-RTC PCR device was successfully fabricated using PS-laser-ablated MLG films and employed in BKV DNA amplification. The LAG technique demonstrated the one-step manufacturing thin-film PCR. The feasibility of the device was determined on the basis of temperature control in sequential experiments, which revealed significantly more rapid amplification of BKV DNA. The hole-array graphene-based heaters displayed stable and uniform temperature distribution. The MLG thin film could be ablated from the glass substrate with minimal ablation damage, a fluence of 4.72 J/cm^2, a repetition rate of 300 kHz, and a scanning speed of 500 mm/s to form the HA-RTC PCR device. Moreover, surface property of MLG PCR device with hydrophilic pattern sites here was required to be the use of forensic DNA evidence. The BKV marker could complete the diagnosis through PCR amplification of a 354-bp VP1 fragment in 70 min on this on-chip device, proving that the heating device fabricated with MLG thin film-based electrodes had satisfactory thermal characteristics with a stable temperature cycle using a programmable control system. For the feasibility of the BKV clinical test, the results revealed that the HA-RTC PCR device could be used for low-cost, rapid, easy-to-use gene testing in environmental and medical fields. The proposed setup platform offers a solution for accurate and portable POC PCR devices for diagnostic purposes.

Acknowledgments

The authors gratefully acknowledge the support of the Ministry of Science and Technology of Taiwan, Republic of China under grant MOST 106-2221-E-003-037, MOST 107-2221-E-003 -006-MY2, MOST 107-2811-E-003-502, and MOST108-2622-E-003-001-CC3.

References

Ahsan, N., Shah, K.V., 2006. Adv. Exp. Med. Biol. 577, 1–18.
Barraclough, K.A., Isbel, N.M., Staatz, C.E., Johnson, D.W., 2011. J. Transplant 750836.
Bigham, S., Fazeli, A., Moghaddam, S., 2017. Sci. Rep. 7, 44745.
Cardoso, A.R., Marques, A.C., Santos, L., Carvalho, A.F., Costa, F.M., Martins, R., Sales, M.G.F., Fortunato, E., 2019. Biosens. Bioelectron. 124–125, 167–175.
Chang, T.L., Chen, Z.C., 2015. Appl. Surf. Sci. 374, 543–549.
Chang, T.L., Chen, Z.C., Lee, Y.W., Li, Y.H., Wang, C.P., 2016. Microelectron. Eng. 158, 95–101.
Chang, T.L., Chou, C.Y., Wang, C.P., Teng, T.C., Han, H.C., 2019. Microelectron. Eng. 210, 19–26.
Cheng, C., Wang, S., Wu, J., Yu, Y., Li, R., Eda, S., Chen, J., Feng, G., Lawrie, B.J., Hu, A., 2016. ACS Appl. Mater. Interfaces 8, 17784–17792.
Chen, C.Y., Chang, T.L., 2015. Microelectron. Eng. 143, 41–47.
Chen, X., Li, T., Zhai, K., Hu, Z., Zhou, M., 2017. Int. J. Adv. Manuf. Technol. 88, 2727–2733.
Chen, X., Shen, J., 2017. J. Chem. Technol. Biotechnol. 92, 271–282.
Chen, Z.C., 2018. Advanced Laser Processing Technology in Graphene for Applications of Biomolecule Devices. PhD dissertation. National Taiwan Normal University.
Crafton, E.F., Black, W.Z., 2004. Int. J. Heat Mass Transf. 47, 1187–1200.
Dinca, M.P., Gheorghe, M., Aherne, M., Galvin, P., 2009. J. Micromech. Microeng. 19, 065009.
Dong, T., Sparkes, M., Durkan, C., O'Neill, W., 2016. J. Laser Appl. 28, 02202.
Drosten, C., Günther, S., Preiser, W., Werf, S.V.D., Brodt, Hans-Reinhard, Becker, S., Rabenau, S., Panning, M., Kolesnikova, L., Fouchier, R.A.M., Berger, A., Burguière, Ana-Maria, Cinatl, J., Eickmann, M., Escriou, N., Grywna, K., Kramme, S., Manuguerra, Jean-Claude, Müller, S., Rickerts, V., Stürmer, M., Vieth, V., Klenk, Hans-Dieter, Osterhaus, A.D.M.E., Schmitz, H., Doerr, H.W., 2003. N. Engl. J. Med. 348, 1967–1976.
Du, D., Zou, Z., Shin, Y., Wang, J., Wu, H., Engelhard, M.H., Liu, J., Aksay, I.A., Lin, Y., 2010. Anal. Chem. 82, 2989–2995.
Evertsson, U., Monstein, H.J., Johannson, A.G., 2000. APMIS 108, 385–392.
Fijan, S., Šulc, D., Steyer, A., 2018. Int. J. Environ. Res. Public Health 15, 1539–1553.
García, G.M., Bi, Y., Prato, M., Spirito, D., Krahne, R., Konstantatos, G., Moreels, I., 2018. Sol. Energy Mater. Sol. Cells 183, 1–7.
Gjoerup, O., Chang, Y., 2010. Adv. Cancer Res. 106, 1–51.
Gong, H., Ramalingam, N., Chen, L., Che, J., Wang, Q., Wang, Y., Yang, X., Yap, P.H., Neo, C.H., 2006. Biomed. Microdevices 8, 167–176.
Hänichen, P., Bender, A., Voß, B., Roisman, T.G., Stephan, P., 2019. Int. J. Heat Mass Transf. 128, 115–124.

Hao, Y.F., Wang, Y.Y., Wang, L., Ni, Z.H., Wang, Z.Q., Wang, R., Koo, C.K., Shen, Z.X., Thong, J.T.L., 2010. Small 6, 195–200.
Hirsch, H.H., Brennan, D.C., Drachenberg, C.B., Ginevri, F., Gordon, J., Limaye, A.P., Mihatsch, M.J., Nickeleit, V., Ramos, E., Randhawa, P., Shapiro, R., Steiger, J., Suthanthiran, M., Trofe, J., 2005. Transplantation 79, 1277–1286.
Holland, J.L., Louie, L., Simor, A.E., Louie, M., 2000. J. Clin. Microbiol. 33, 4108–4113.
Hryniewiecki, T., Gzyl, A., Augustynowicz, E., Rawczynska-Englert, 2002. J. Heart Valve Dis. 11, 870–874.
Huang, P., Wang, H., Cao, Z., Jin, H., Chi, H., Zhao, J., Yu, B., Yan, F., Hu, X., Wu, F., Jiao, C., Hou, P., Xu, S., Zhao, Y., Feng, N., Wang, J., Sun, W., Wang, T., Gao, Y., Yang, S., Xia, X., 2018. Front. Microbiol. 9, 1101–1109.
Jaenisch, R., Bird, A., 2003. Nat. Genet. 33, 245–254.
Jha, A., Ahmed, W., Pakkyara, A., Shaheen, F., Salmi, I.A., 2018. Saudi J. Kidney Dis. Transpl. 29, 1073–1081.
Jia, J., Sun, L., Hu, N., Huang, G., Weng, J., 2012. Small 8, 2011–2015.
Jin, L., 1993. Mol. Cell. Probes 7, 331–334.
Justino, C.I.L., Gomes, A.R., Freitas, A.C., Duarte, A.C., Rocha-Santos, T.A.P., 2017. Trends Anal. Chem. 91, 53–66.
Karimi, S., Rashidian, E., Birjandi, M., Mahmoodnia, L., 2018. Electron. Physician 10, 6534–6539.
Kim, J., Park, S.J., Min, D.H., 2016. Anal. Chem. 89, 232–248.
Kim, Y., Lee, J., Park, S., 2018. Micromachines-Basel 9, 472–483.
Krumbholz, A., Zell, R., Egerer, R., Sauerbrei, A., Helming, A., Gruhn, B., Wutzler, P., 2006. J. Med. Virol. 78, 1588–1598.
Lee, D.N., Kim, J., Jang, J.G., Hong, J.I., 2017. Sens. Actuators B Chem. 252, 706–711.
Li, B.J., Li, H., Huang, L.J., Ren, N.F., Kong, X., 2016. Appl. Surf. Sci. 389, 585–593.
Liébana, S., Jones, L.J., Drago, G.A., Pittson, R.W., Liu, D., Perrie, W., Hart, J.P., 2016. Sens. Actuators B Chem. 231, 384–392.
Lien, K.Y., Lee, S.H., Tsai, T.J., Chen, T.Y., Lee, G.B., 2009. Microfluid. Nanofluidics 7, 795–806.
Lin, S., Feng, W., Miao, X., Zhang, X., Chen, S., Chen, Y., Wang, W., Zhang, Y., 2018. Biosens. Bioelectron. 110, 89–96.
Liu, B., Salgado, S., Maheshwari, V., Liu, J., 2016. Curr. Opin. Colloid Interface Sci. 26, 41–49.
Liu, Z., Chen, Z., Yu, F., 2018. Sol. Energy Mater. Sol. Cells 174, 453–459.
Low, S.S., Tan, M.T.T., Loh, H.S., Khiew, P.S., Chiu, W.S., 2016. Anal. Chim. Acta 903, 131–141.
Mackay, I.M., Arden, K.E., Nitsche, A., 2002. Nucleic Acids Res. 30, 1292–1305.
Mackenzie, D.M.A., Buron, J.D., Whelan, P.R., Jessen, B.S., Silajdźić, A., Pesquera, A., Centeno, A., Zurutuza, A., Bøggild, P., Petersen, D.H., 2015. 2D Mater. 2, 045003.
McCabe, K.M., Khan, G., Zhang, Y.H., Mason, E.O., McCabe, E.R., 1995. Pediatrics 95, 165–169.
Moschou, D., Vourdas, N., Kokkoris, G., Papadakis, G., Parthenios, J., Chatzandroulis, S., Tserepi, A., 2014. Sens. Actuators B Chem. 199, 470–478.
Neuzil, P., Pipper, J., Hsieh, T.M., 2006. Mol. Biosyst. 2, 292–298.
Ngo, C.V., Chun, D.M., 2017. Appl. Surf. Sci. 409, 232–240.
Nieto, D., McGlynn, P., Fuente, M.D.L., Lopez-Lopez, R., O'connor, G.M., 2017. Colloids Surfaces B Biointerfaces 154, 263–269.
Niu, X., Zheng, W., Yin, C., Weng, W., Li, G., Sun, W., Men, Y., 2017. J. Electroanal. Chem. 806, 116–122.
Petralia, S., Conoci, S., 2017. ACS Sens. 2, 876–891.
Rethfeld, B., Ivanov, D.S., Garcia, M.E., Anisimov, S.I., 2017. J. Phys. D Appl. Phys. 50, 193001.
Riera, S., Barrau, J., Rosell, J.I., Omri, M., Fréchette, L.G., 2013. Experimental demonstration of a tailored-width microchannel heat exchanger configuration for uniform wall temperature. J. Phys. Conf. Ser. 476, 012075.
Saiki, R.K., Gelfand, D.H., Stoffel, S., Scharf, S.J., Higuchi, R., Horn, G.T., Mullis, K.B., Erlich, H.A., 1988. Science 239, 487–491.
Sawinski, D., Goral, S., 2015. Nephrol. Dial. Transplant. 30, 209–217.
Seo, H., Lim, Y., Shin, H., Bang, I.C., 2018. Int. J. Heat Mass Transf. 120, 587–596.
Seo, H., Yun, H.D., Kwon, Soon-Yong, Bang, I.C., 2016. Nano Lett. 16, 932–938.
Shenagari, M., Monfared, A., Eghtedari, H., Pourkazemi, A., Hasandokht, T., Khosravi, M., Asharfkhani, B., 2017. J. Clin. Virol. 96, 7–11.
Sugioka, K., Cheng, Y., 2014. Light Sci. Appl. 3, e149.
Suvarnaphaet, P., Pechprasarn, S., 2017. Sensors 17, 2161–2184.
Tan, S.K., Huang, C.H., Sahoo, M.K., Weber, J., Kurzer, J., Stedman, M.R., Concepcion, W., Gallo, A.E., Alonso, D., Srinivas, T., Storch, G.A., Subramanian, A.K., Tan, J.C., Pinsky, B.A., 2019. J. Infect. Dis Published in Mar 14.
Thiha, A., Ibrahima, F., Muniandy, S., Dinshawc, I.J., Teha, S.J., Thong, K.L., Leo, B.F., Madou, M., 2018. Biosens. Bioelectron. 107, 145–152.
Ugsornrat, K., Afzulpurkar, N.V., Wisitsoraat, A., Tuantranont, A., 2010. Sens. Mater. 22, 271–284.
Vanegas, D.C., Patiño, L., Mendez, C., Oliveira, D.A.D., Torres, A.M., Gomes, C.L., McLamore, E.S., 2018. Biosensors 8, 42–60.
Verma, A.K., Das, R., Soni, R.K., 2018. Appl. Surf. Sci. 427, 133–140.
Wang, W., Li, Q., Yang, X., Wang, K., Du, S., Zhang, H., Nie, Y., 2016. Biosens. Bioelectron. 77, 1001–1007.
Wang, Y., Wang, F., Wang, H., Song, M., 2017. Sci. Rep. 7, 16510.
Winter, J., Rapp, S., Schmidt, M., Huber, H.P., 2017. Appl. Surf. Sci. 417, 2–15.
Wu, Y., Zhang, X., Zhang, X., 2016. Appl. Therm. Eng. 99, 938–943.
Yamamoto, M., Kimura, H., Hironaka, T., Hirai, K., Hasegawa, S., Kuzushima, K., Shibata, M., Morishima, T., 1995. J. Clin. Microbiol. 33, 1765–1768.
Yin, W.Y., Lee, M.C., Lai, N.S., Lu, M.C., 2015. J. Formos. Med. Assoc. 114, 373–374.
Zang, Z., Zeng, X., Wang, M., Hu, W., Liu, C., Tang, X., 2017. Sens. Actuators B Chem. 252, 1179–1186.